Shear-Thinning Nanocomposite Hydrogels for the Treatment of Hemorrhage

Akhilesh K. Gaharwar,[†,‡,§,∥,⊥,¶] Reginald K. Avery,[#,§] Alexander Assmann,[⊗,§,‡,⊥] Arghya Paul,[‡,§,⊥,∞] Gareth H. McKinley,[▽] Ali Khademhosseini,[*,§,‡,⊥] and Bradley D. Olsen[*,†]

[†]Department of Chemical Engineering, Massachusetts Institute of Technology, Cambridge, Massachusetts 02139, United States, [‡]Wyss Institute for Biologically Inspired Engineering, Harvard University, Boston, Massachusetts 02115, United States, [§]Center for Biomedical Engineering, Department of Medicine, Brigham and Women's Hospital, Harvard Medical School, Cambridge, Massachusetts 02139, United States, [⊥]Harvard-MIT Division of Health Sciences and Technology, Massachusetts Institute of Technology, Cambridge, Massachusetts 02139, United States, [∥]David H. Koch Institute for Integrative Cancer Research, Massachusetts Institute of Technology, Cambridge, Massachusetts 02139, United States, [#]Department of Biological Engineering, Massachusetts Institute of Technology, Cambridge, Massachusetts 02139, United States, [▽]Department of Mechanical Engineering, Massachusetts Institute of Technology, Cambridge, Massachusetts 02139, United States, and [⊗]Department of Cardiovascular Surgery, Heinrich Heine University, Medical Faculty, 40225 Duesseldorf, Germany. [¶]Present address: Department of Biomedical Engineering, Texas A&M University, College Station, TX 77843. [∞]Present address: Department of Chemical & Petroleum Engineering, School of Engineering, University of Kansas, 1530 W. 15th St., Lawrence, KS, 66045-7609, USA.

ABSTRACT Internal hemorrhaging is a leading cause of death after traumatic injury on the battlefield. Although several surgical approaches such as the use of fibrin glue and tissue adhesive have been commercialized to achieve hemostasis, these approaches are difficult to employ on the battlefield and cannot be used for incompressible wounds. Here, we present shear-thinning nanocomposite hydrogels composed of synthetic silicate nanoplatelets and gelatin as injectable hemostatic agents. These materials are demonstrated to decrease *in vitro* blood clotting times by 77%, and to form stable clot-gel systems. *In vivo* tests indicated that the nanocomposites are biocompatible and capable of promoting hemostasis in an otherwise lethal liver laceration. The combination of injectability, rapid mechanical recovery, physiological stability, and the ability to promote coagulation result in a hemostat for treating incompressible wounds in out-of-hospital, emergency conditions.

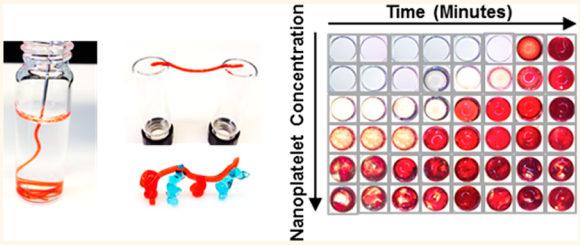

KEYWORDS: nanocomposites · hydrogels · synthetic silicate nanoplatelet · shear thinning · hemorrhage

A range of hemostats have been reported that decrease the time required to establish hemostasis by dehydrating the injury site,[1,2] concentrating clotting factors,[2,3] delivering clotting agents (such as thrombin and fibrinogen)[1,2,4] or forming a physical barrier against bleeding,[5] to the injured site to promote clotting. However, most of these hemostats are suitable for external wounds,[6,7] where hemostatic agents and external pressure can be applied simultaneously. Recently, thrombin and fibrinogen-based injectable solutions have been developed, but these injectable solution-based hemostats pose the risk of introducing strong coagulation activators into the circulatory system.[8,9] Therefore, there is a need for new hemostatic biomaterials that are injectable into a wound, mechanically stable, and induce rapid and local hemostasis.

One approach to developing hemostatic agents for traumatic injuries is to engineer injectable biomaterials that can be introduced into a wound site, forming a physiologically stable artificial matrix and promoting the natural clotting cascade. Specifically, the biomaterial should flow with minimal applied pressure during injection, providing a method of application that avoids additional patient trauma. However, once in the wound, the material should solidify to prevent biomaterial loss to unaffected areas. Shear-thinning hydrogels can satisfy these requirements and have been developed from a wide variety of material platforms.[10,11]

Multiple approaches have been developed to incorporate functional materials into hemostats to enhance their therapeutic properties. These include commercial

* Address correspondence to bdolsen@mit.edu, alik@rics.bwh.harvard.edu.

Received for review July 8, 2014 and accepted September 15, 2014.

Published online September 15, 2014
10.1021/nn503719n

products such as QuikClot that incorporate kaolin, a crystalline mineral that functions as an absorbent and coagulation activator.[12] Floseal uses gelatin and thrombin to promote clotting in an injectable form.[8] An emerging approach to integrate functionality into hydrogel networks focuses on incorporating nanoparticles.[13−17] Nanomaterials have been shown to interact with blood to promote clotting *via* mechanisms such as platelet activation, dehydration of the plasma, delivery of coagulating factors, formation of physical barriers, or the activation of clotting factors.[1,18−22]

Highly charged nanoparticles, such as synthetic silicate nanoplatelets, have been shown to induce blood coagulation by concentrating clotting factors.[4] Synthetic silicates are charged disks, 20−30 nm in diameter and ~1 nm in thickness.[23] Due to the anisotropic distribution of their surface charge, positive along the edge and negative on the top and bottom surfaces, the nanoplatelets can form self-assembled structures which can dynamically form and break, creating shear thinning gels when in aqueous media.[24] Recently, synthetic silicate nanoplatelets have been used as osteogenic agents,[23] drug delivery agents,[25] tissue engineered scaffolds,[26−29] solid hemostat products,[4,30,31] additives in cosmetic creams,[32,33] and rheological modifiers.[34] Synthetic silicates such as Laponite are shown to degrade into nontoxic components (Na^+, Mg^{2+}, $Si(OH)_4$, Li^+) in physiological conditions.[35] Moreover, these silicates are found to be cytocompatible with human stem cells and animal cells as reported in previous literature.[23,26,28]

Natural and synthetic polymers have been shown to interact with synthetic silicates through physical interactions, forming physically cross-linked networks.[26,28,29,36,37] Earlier studies on silicate−gelatin interactions show that polyampholytic gelatin, containing positive and negative regions, strongly interacts with the oppositely charged areas of the synthetic silicate nanoplatelets.[38] Gelatin is denatured collagen, and mimics components of the native extracellular matrix (ECM) in structure and chemical composition.[39] Gelatin's hygroscopic property also allows for absorption of body fluids and is proposed for a range of tissue engineering applications.

RESULTS/DISCUSSION

Characterization of Nanocomposites. Physical mixtures of gelatin and silicate nanoplatelets were used to formulate the nanocomposite hydrogels for this study. Briefly, the silicate nanoplatelets were exfoliated in ultrapure (Milli-Q) water using a vortexer to enhance the surface area available for interaction with gelatin. Next, a gelatin stock, heated to liquefy the solution, was vigorously mixed with the exfoliated silicate at room temperature (Figure 1a). Vigorous agitation was necessary to prevent clumping of the nanoplatelets during gelation; however, the nanoplatelets are stably dispersed after the gel has set.[24] Nanocomposite hydrogels were fabricated with solid concentrations of 3, 6, and 9 wt % and gelatin/nanoplatelet ratios from 0:1 to 1:0 and labeled as *x*NC*y* ("*x*" represents the total solid weight percent and "*y*" is percent of the total solid weight percent that is nanoplatelet) (Supporting Information, Table S1). Initially, the gelatin solution was a viscous liquid (at 37 °C), but once silicate nanoplatelets were mixed with gelatin, the solution gelled within a minute.

When mixed with gelatin, silicate nanoplatelets improved the thermal stability of the hydrogel. Thermal stability of the nanocomposite formulations was determined by oscillatory shear rheology over a temperature range from 15 to 45 °C, mimicking common environmental and physiological temperatures that the nanocomposite may be exposed during sample preparation and *in vivo* application. 9NC0 had a gel−sol transition temperature of 32 °C (Supporting Information, Figure S1), consistent with the literature and too low for application as a hemostat.[40] However, the addition of silicate nanoplatelets to gelatin improved the thermal stability, increasing the sol−gel transition to above 45 °C for solids concentrations of 6 wt % or greater. In contrast, 3 wt % solids nanocomposites were not solid within the experimentally observed temperature range. For treatment of hemorrhage, thermal stability is necessary once the nanocomposite is injected so that it can remain at the wound site without flowing into adjacent areas. Similarly, physiological stability was observed for all 9 wt % nanocomposites, 6NC50, 6NC75, and 6NC100 (Supporting Information, Figure S2). All gelatin samples, quickly dissolved in PBS at 37 °C while the aforementioned samples had no observed weight loss over 24 h. For this reason, only nanocomposite hydrogels with more than 6 wt % solids were characterized further.

Zeta potential measurements suggest that electrostatic interactions between nanoplatelets and gelatin contributed to the observed increase in the thermal stability (Figure 1b). Solutions of silicate nanoplatelets possessed a zeta potential of −39 mV, whereas gelatin solutions had a zeta potential of 10 mV. Because the two components had opposite charges, electrostatic interactions between silicate and gelatin were expected. This was also supported by earlier findings which showed that strong interactions between montmorillonite (another type of silicate clay) and gelatin can function to increase the sol−gel transition temperature of the composite.[41]

Scattering measurements of nanocomposite hydrogels suggest the presence of disk shaped particles, indicating that clay particles remain exfoliated in the nanocomposite. Small angle X-ray scattering (SAXS) intensity curves of the nanocomposites showed power law decay with an exponent of −2 at high q, greater than 0.03 $Å^{-1}$, characteristic of disk-shaped scatterers. The scattering intensity from 9NC75 can be fit with a

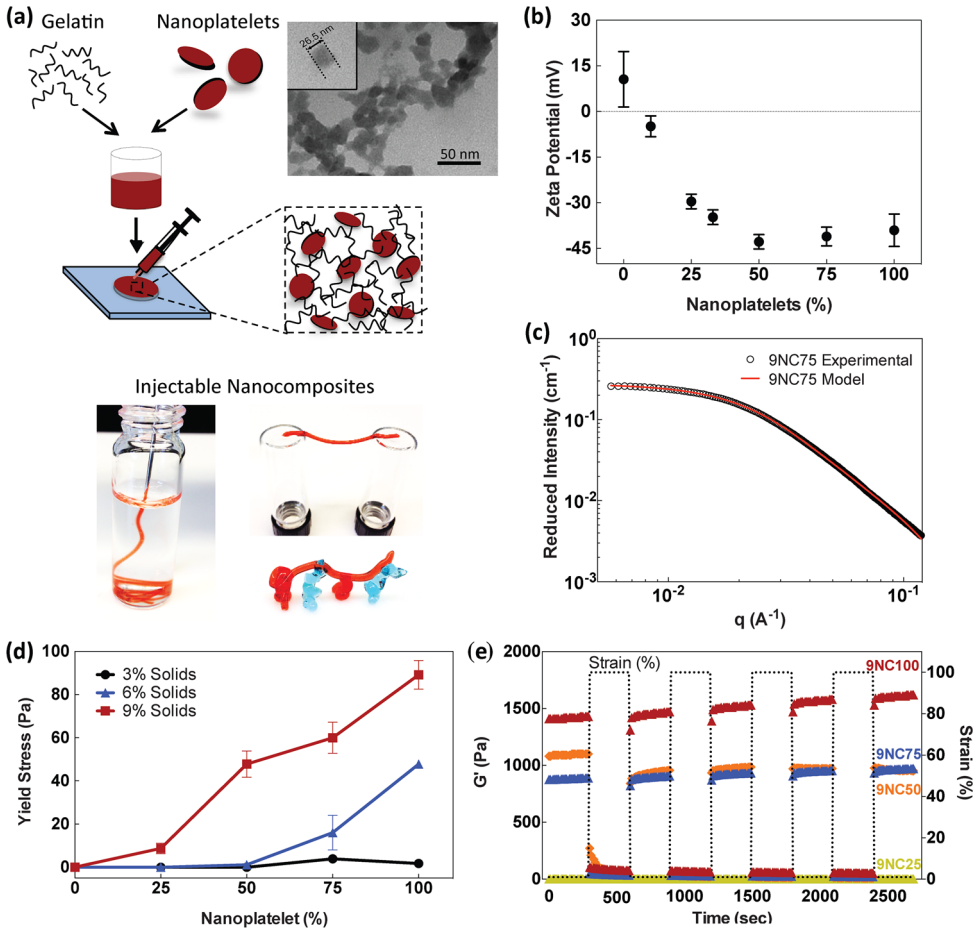

Figure 1. Structure, injectability, and self-healing characteristics of nanocomposite hydrogels. (a) Schematic showing the preparation of the nanocomposite gels. The TEM image shows the size of the silicate nanoparticle (scale bar 50 nm). Images showing injection of nanocomposite hydrogel through a surgical needle (22 gauge) and recovery to form freestanding structures. (b) Zeta potential measurements demonstrate electrostatic interactions between negatively charged silicate and positively charged gelatin; 95% CI are shown for each point. (c) Small-angle X-ray scattering (SAXS) indicates that nanoplatelets are well dispersed and follow the model curve for scattering from dispersed thin disks. (d) Yield stress of gels as a function of nanoplatelet loading and solids fraction. (e) Recovery of the nanocomposites was observed by subjecting the hydrogel to alternating high and low strain conditions (100% strain and 1% strain) while monitoring the moduli of the composite. For all the nanocomposite hydrogels, more than 95% recovery was observed.

thin disk model[42] with a radius of 9.5 ± 2.7 nm, in agreement with the reported size of the silicate nanoplatelets (Figure 1c).[23] This suggests that scattering was produced from individual nanoplatelets dispersed within the gelatin in this formulation and not aggregates of nanoplatelets (Supporting Information, Figure S3).

Silicate addition to gelatin modulated the rheological response of the nanocomposite, resulting in a shear yielding behavior observed at 37 °C. Preliminary investigations using a 22-gauge needle indicated that all silicate-containing nanocomposite hydrogels could be injected and form self-supporting structures, suggesting the presence of a yield stress and recovery potential (Figure 1a). Linear oscillatory shear rheology showed that the crossover frequency was below 0.001 Hz for 9NC75 and 9NC100, maintaining solid-like ($G' > G''$) properties over the tested frequency range (Supporting Information, Figure S4). Oscillatory strain into the nonlinear regime (Supporting Information, Figure S4) illustrated yielding behavior, an important parameter for designing hydrogels for minimally invasive therapies. In oscillatory shear rate sweeps, the yield stress was defined as a 5% departure of the stress from the initial linearity on a stress–strain plot. Tests were performed at 37 °C, where gelatin readily flows and lacks a yield stress (Figure 1d; Supporting Information, Figure S4). An increase in the silicate concentrations from 0% (9NC0) to 100% (9NC100) increased the yield stress from 2 to 89 Pa. A yield stress was observed in 9NC100 but not in 9NC0, suggesting that the yield stress behavior was derived from the presence of the dispersed nanoplatelets in the nanocomposite, consistent with the known shear thinning capability of nanoplatelets.[40] Because increasing concentration of gelatin reduces the yield stress, it eases delivery of the nanocomposite by injection.

Recovery of the elastic gel strength in less than 10 seconds was observed in nanocomposites for

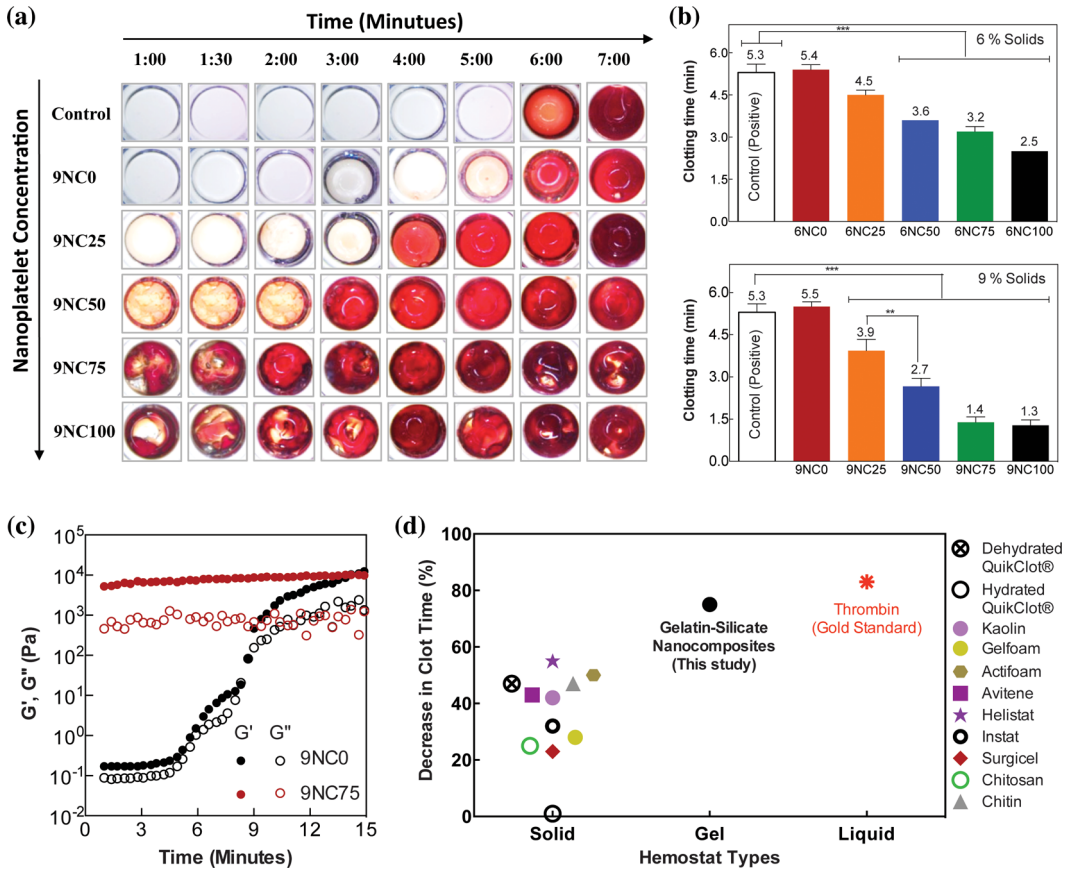

Figure 2. Effect of nanoplatelets on the clotting whole blood. (a) Clot formation as a function of time and nanocomposite composition. (b) Quantiative clot times for 6% and 9% nanocomposites. (One-way Anova followed by Tukey's post-hoc analysis was performed; *$p < 0.01$; ***$p < 0.001$). (c) Clotting kinetics of blood when in contact with gelatin and nanocomposite monitored using shear rheology. (d) Comparison of clotting times for silicate-gelatin nanocomposite (NC) and commercial products.

nanoplatelet loadings greater than 50% (9NC50, 9NC75, and 9NC100). Such rapid self-healing after the removal of stress can prevent material flow after application to a wound site. Other physically cross-linked hydrogels are capable of recovering their prestrained moduli in seconds (*i.e.* telechelic protein gels)[43] to tens of minutes (*i.e.* peptide amphiphile gels)[5] after the cessation of shear. Therefore, the rapid recovery time of these gels provides a significant advantage by reducing the risk being washed away because they have relatively long self-healing times after the deformation of physically cross-linked networks.[5] Figure 1e shows four cycles of high (100%) to low (1%) oscillatory strain amplitudes and the resulting nanocomposite moduli. At 100% oscillatory strain, all apparent moduli are below 100 Pa by the end of 5 minutes of oscillation, illustrating rapid network disruption. After four cycles of high and low oscillatory strain, the 9NC50 modulus during 100% strain oscillations was 80% lower than the initial modulus during high strain. At higher silicate loading (9NC75 and 9NC100), the moduli were 33% and 29% lower compared to the initial values during high strain. In contrast, the moduli for the high nanoparticle materials increased under quiescent conditions. While 9NC50 showed a 13.5% decrease after four strain cycles, 9NC75 and 9NC100 showed 9.3% and 13.3% increases in modulus, respectively. Extended monitoring (Supporting Information, Figure S5) indicated that after 30 seconds the quiescent moduli reached asymptotic values, indicating completion of the healing process. These results indicate rapid recovery of the storage modulus after repeated application of high oscillatory strain amplitudes, suggesting rapid recovery of the physically cross-linked networks.

***In Vitro* Performance of Nanocomposite in the Presence of Whole Blood.** The incorporation of silicate nanoplatelets into gelatin led to a decrease in the observed clotting time *in vitro*. The hemostatic ability of nanocomposite hydrogels was evaluated by monitoring the clotting time of whole blood in contact with the nanocomposite surfaces in 96-well plates. Under normal conditions, human blood initiates coagulation in 5−6 min.[4,44] Similar clotting times (5.2 ± 0.5 min) for whole blood were observed in control wells containing neither gelatin nor nanocomposite (Figure 2a,b). A slight color change was observed in 9NC0 by 5 min. This was attributed to the tamponade ability of gelatin.[45] Gelatin is hygroscopic and could absorb

the fluid components of whole blood but could not stimulate clot formation within 5 min. The addition of nanoplatelets to gelatin reduced blood clotting time in a dose-dependent manner. Figure 2a,b demonstrates the decreased clotting time for higher nanoplatelet concentrations. 9NC25, 9NC50, and 9NC75 reduced the clotting time by 32%, 54%, and 77%, respectively, when compared to the control (blood in uncoated wells). The representative images of wells at select time points, shown in Figure 2a, clearly highlight the presence of a clot earlier in nanocomposites with higher nanoplatelet loadings. This was attributed to the strong negative charge of the synthetic silicate nanoplatelet that can facilitate concentration of clotting factors near the nanocomposite surface. Prior studies have shown a decrease in clotting time due to the addition of negatively charged particles to polymer hydrogels.[4,12] Preliminary *in vitro* studies indicate that the nanocomposites induced minimal cytotoxic effect or inflammatory response (Supporting Information, Figure S6), with gelatin-containing nanocomposites having higher cell viability and lower inflammatory response than NC100 gels, supporting the potential application of these materials as biocompatible hemostatic gels.

Decreased clotting times of blood in contact with nanocomposites were also observed through rheological measurements. Small amplitude oscillatory time sweeps of blood in contact with gelatin or gelatin–silicate nanocomposites were performed to evaluate clotting kinetics (Figure 2c. Gelatin was chosen as a control, having minimal impact on clotting time *in vitro*. 9NC75 was selected for its combination of decreased clotting time, comparable to 9NC100 which was the best performer *in vitro*, and its decreased inflammatory response when compared to 9NC100, insignificant from the inflammatory response of 9NC0 (Supporting Information, Figure S6). Clotting induced an increase in the elastic modulus of the gelatin-clot system from 10^{-1} to 10^{4} Pa (Figure 2c). Whole blood in contact with gelatin begins cloting in 5–7 min, which is consistent with our earlier clotting data and the literature.[46] When gelatin was replaced with a silicate–gelatin nanocomposite, the clotting transition occurred even prior to the initiation of measurements, reflecting a large reduction in the clotting time. Comparing the decrease in clotting time observed with nanocomposites to other reported hemostatic products, the improvement exceeds many solid hemostats and was similar to recorded values for thrombin-based hemostats (Figure 2d).[4,6,46,47] A comparison of the nanocomposite and the commercial hemostat QuikClot clot mass per contact area as a function of time showed similar trends in clot formation (Supporting Information, Figure S7).

Blood clot strength was preserved in blood-nanocomposite systems. Clot strength, characterized by the peak shear stress attained in a linearly increasing strain experiment, is a parameter important for establishing hemostasis. More rigid clots are more likely to embolize while more pliable clots are ineffective. Stress–strain curves of each system were compared to a natural clot under the same testing conditions. The results indicate that the clot could sustain a peak shear stress of 2.4 $\pm$ 0.3 kPa, while the gelatin-clot system had a peak shear stress of 0.5 kPa (Supporting Information, Figure S8). The liquid-like properties of gelatin ($G'' > G'$) at 37 °C compromise the mechanical stability of the system. Nanocomposites tested under the same conditions reached a maximum shear stress of 1.0 $\pm$ 0.09 kPa. In the presence of nanocomposite, the shear stress of a nanocomposite-clot was 1.9 $\pm$ 0.6 kPa, which is comparable to the peak stress borne by the clot.

It was hypothesized that the surface charge of the nanocomposite facilitated platelet aggregation or activation of clotting factors that ultimately enhanced the hemostatic activity. To confirm this, a channel was generated within the nanocomposite hydrogels and subsequently filled with blood. It was observed that platelets aggregated near the nanocomposite surface (Supporting Information, Figure S9), which was not observed in control experiments on gelatin or plastic surfaces. This indicates that nanocomposite surfaces might be effective in attracting blood components.

Observations in the presence of platelet rich plasma (PRP) and platelet poor plasma (PPP) (Supporting Information, Figure S9) indicated that components in both plasma types were colocalized with silicates, forming aggregates around the silicates. This colocalization and protein adsorption to the nanocomposite surfaces could be driven by electrostatic or hydrophobic interactions, which have been shown to determine protein adsorption to biomaterial surfaces.[48,49] The first row of images in Supporting Information, Figure S9 shows a uniform fluorescence from a silicate nanoplatelet solution. The second row (whole blood) shows blood cells with a minimal fluorescent signature. The mixture of labeled 9NC100 and PPP showed colocalization of the plasma components with the silicate nanoplatelets (third row). The same was observed for the nanoplatelets and PRP (fourth row). The uniform fluorescence of the nanoplatelets is disrupted by the presence of blood components, suggesting a change in the interactions between nanoplatelets. The colocalization of silicates and blood components is thought to originate from plasma proteins and blood cells interacting with the charged surfaces of silicate nanoplatelets, increasing blood component concentrations surrounding the nanocomposite. Earlier studies have shown that charge interactions can initiate the coagulation cascade, such as the interactions of GPIb-V receptors (negative) with platelets and von Willebrand factor (positive) with collagen.[20,50,51] The attractive properties of the silicates could serve to accelerate

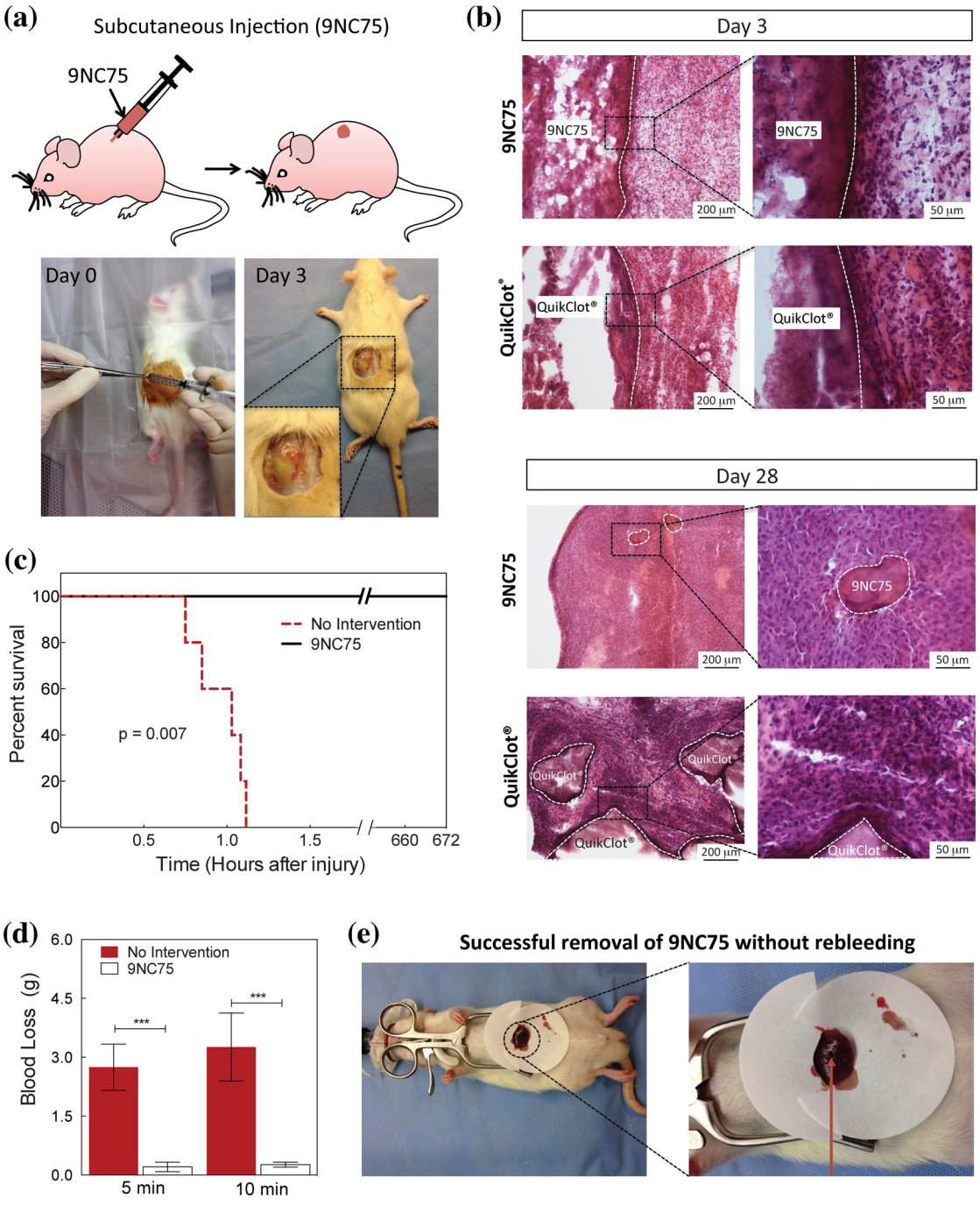

Figure 3. ***In vivo*** **evaluation of nanocomposite hydrogels as hemostats. (a) Subcutaneous injection and explantation of 9NC75 in rats. After 3 days, nanocomposite could be easily detected in the subcutaneous pockets, but the volume was already lower than at implantation. (b) H&E staining confirmed degradation of 9NC75 within 28 days, while the QuikClot particles were still present. Moreover, 9NC75 induced less chronic inflammation than QuikClot, indicated by severe mononuclear cell infiltration around QuikClot at day 28 (asterisks). Furthermore, the QuikClot samples were encapsulated by dense fibrous connective tissue (arrows). The potential of the nanocomposite to stop otherwise lethal bleeding was investigated using liver bleeding experiments in rats. (c) 9NC75 significantly improved the postinterventional survival (logrank (Mantel-Cox) test). (d) 9NC75 was effective in preventing blood loss as compared to untreated hemorrhage (*** $p < 0.001$). (e) The small amount of 9NC75 (200 μL) was sufficient to stop bleeding and the superficial part of the 9NC75 was easily removed without causing rebleeding.**

hemostasis, with similar protein−nanocomposite interactions observed in other hemostats.[47]

In Vivo **Hemostatic Potential of Nanocomposite in Liver Bleeding Model.** *In vivo* biocompatibility of nanocomposite hydrogels was investigated by dorsal subcutaneous injection in rats *via* 1 cm incisions. 9NC75 (200 μL) or QuikClot samples (200 μL) were injected or implanted, respectively, in subcutaneous pockets ($n = 16$) as shown in Figure 3a. All animals survived the follow-up period of 28 days without any signs of physical impairment or systemic inflammation, and exhibited regular somatic growth. After 3 days, both implant materials (9NC75

and QuikClot) could be easily detected in the subcutaneous pockets. At day 28, the QuikClot particles appeared macroscopically unchanged and 9NC75 was integrated in the surrounding tissue. Hematoxylin & Eosin (H&E) staining confirmed these observations indicating that 9NC75 was predominantly degraded within 28 days after injection, while QuikClot did not undergo degradation (Figure 3b).[52] Both implants induced an acute locally restricted inflammatory reaction in the host, including cellular infiltration. This process turned into chronic inflammation of the surrounding tissue, whereas the inflammatory response against QuikClot was substantially stronger when compared to 9NC75, resulting in a higher density and larger area of predominantly mononuclear cellular infiltrates. Moreover, in the QuikClot group, dense fibrous tissue formation was detected around the implants at day 28, indicating fibrous capsule formation (Figure 3b).

To investigate the potential of the nanocomposite to stop otherwise lethal bleeding, a standardized liver bleeding model was applied (Supporting Information, Figure S10). In the liver bleeding experiments (n = 12 rats), median laparotomy was performed, and the central liver lobe was exposed. After draping of the surrounding *situs* with filter paper for blood collection, a circular liver laceration (1 cm diameter) with standardized shape and size was created. Immediately after the injury, 9NC75 or QuikClot was applied on the site of lesion. The principal lethality of this bleeding model was assessed in control animals (n = 5) without application of a hemostat. Both 9NC75 (n = 5) and QuikClot (n = 2) were effective in stopping relevant hemorrhage within seconds and prevented hypovolemic conditions. A log rank analysis of the early postinterventional survival data revealed significant improvement by the nanocomposite (logrank (Mantel-Cox) test: p = 0.007 *versus* control; hazard ratio 11.5 with 95% CI 1.93−68.9) (Figure 3c). The total blood loss after 5 and 10 minutes was significantly decreased by the application of 9NC75 ($p < 0.001$ *versus* control) (Figure 3d). The small amount of applied nanocomposite (200 μL) was more than sufficient, since the superficial parts of the nanocomposite were not soaked with blood, and thorough removal of this excess material did not cause rebleeding (Figure 3e). All hemostat-treated liver bleeding animals survived the complete follow-up period of 28 days without secondary hemorrhage. At explantation, no remnants of the nanocomposite were observed and the liver presented an intact surface, while QuikClot was still present, accompanied by soft tissue adhesion to the site of lesion. These results show that the nanocomposite gel offers a strong hemostatic potential for *in vivo* applications and is suitable to stop lethal bleeding.

CONCLUSION

In conclusion, nanocomposite hydrogels containing synthetic silicate disks and gelatin form injectable biomaterials that can promote *in vitro* and *in vivo* coagulation. The addition of silicate nanoplatelets to gelatin significantly improved the physiological stability, injectability, hemostatic performance, and nanocomposite-clot strength. Future studies into the long-term effects of the nanocomposite *in vivo* will be required in any translational applications. In addition, the ability of the nanocomposite to be used as a delivery vehicle for additional clotting or regenerative signaling molecules will be an area for continued investigation. Due to these unique features, the newly developed silicate based gelatin nanocomposite can be used as an injectable hemostat to treat incompressible wounds.

METHODS

Materials. Synthetic silicate nanoplatelets (Laponite XLG) were purchased from Southern Clay Products, Inc. (Louisville, KY). Type-A porcine skin gelatin was obtained from Sigma-Aldrich (Milwaukee, WI). Zeta potentials of gelatin, silicate nanoplatelet, and mixtures of silicate and gelatin were determined in ultrapure water (Milli-Q) and phosphate buffered saline (PBS), pH 7.4 (Invitrogen) using a 633 nm laser in a Malvern ZEN3600 (Malvern Instruments, U.K.). Silicate nanoplatelets were dissolved with vigorous agitation (vortexing) while gelatin was dissolved with stirring at 40 °C. Transmission election microscopy (TEM) images of the silicate nanoplatelets were obtained using a JEOL JEM-1400 TEM (JEM1400) installed with a cool beam illumination system (resolution: 0.2 nm line, 0.38 nm point) and 11 megapixel Advanced Microscopy Techniques cooled charged coupled device camera at 80 kV. The sample was prepared by dispersing silicate nanoplatelets in water/ethanol solutions, placing a drop on the TEM grid, and allowing the grid to dry under vacuum.

Nanocomposite Formulation. Stock solutions of 18% (w/w) gelatin and 9, 6, or 3% (w/w) nanoplatelets were prepared in water (Supporting Information Table S1). Milli-Q water was heated to 40 °C to dissolve gelatin. Water (4 °C) was used for nanoplatelet stock solutions to retard the gelation and allow for full dissolution of nanoplatelet particles prior to gelling. The nanoplatelet gels were allowed to sit at room temperature to fully hydrate until a clear gel was formed. The nanocomposite compositions were made by vortexing the gelatin stock, nanoplatelet stock, and Milli-Q water at 3000 rpm for 5 min to achieve the correct solid concentration and nanoplatelet loading. Nanocomposites were again heated and vortexed. The nanocomposites were then stored at 4 °C.

Nanocomposite Degradation. Nanocomposite samples were placed in 2.0 mL Eppendorf tubes and weighed. Each sample was centrifuged in a swinging bucket rotor centrifuge to obtain a flat interface. Each sample was soaked in phosphate buffered saline (pH 7.4; Invitrogen), stored at 37 °C. At set times, the PBS was removed, and the nanocomposite reweighed. The change in weight was recorded up to 24 h after initial soaking. PBS was replaced after each weighing.

Rheological Analysis. An Anton Paar MCR 301 rheometer was used for mechanical testing. A 25 mm diameter parallel plate geometry with a gap height of 500 μm was used for temperature sweeps and mineral oil was placed around the circumference of the plate to prevent evaporation of water from the nanocomposite for all tests. Nanocomposites were equilibrated

for 10 min prior to testing, followed by a 2 min steady shear at 10 s^{-1}. This was enough time to allow the viscosity to reach a minimum, shear thinning the hydrogel and removing the mechanical history. Ten seconds of equilibrium time was sufficient for the viscosity to return to a higher plateau value, after which point testing was initiated. Frequency and shear rate sweeps were performed at 20 and 37 °C, sweeping frequencies from 0.001 to 100 Hz at 1% strain and shear rates from 0.001 to 100 s^{-1} with 10 points/decade. Frequency sweeps were performed with a cone geometry (25 mm diameter, 1° angle, 50 μm truncation gap). Stress-controlled temperature sweeps were performed from 15 to 45 °C at 10 Pa stress and 1 Hz. All other tests were performed at 37 °C. Oscillatory stress sweeps were performed from 0.01 to 100 Pa at 1 Hz. Strain sweeps were performed from 0.01 to 1000% at 1 Hz. Recovery testing was conducted at 1 Hz by applying 100% strain, a value outside of the linear viscoelastic range, followed by 1% strain for 5 min to monitor gel recovery. Interfacial strength was also measured by applying a linearly increasing strain to a system of nanocomposite and coagulated blood. Shear stress was measured until 1800% strain. The maximum stress attained was used as a measure of the strength of the clot system.

Clotting Time Assay. A volume of 630 μL citrated blood was pipetted into a 1.5 mL Eppendorf tube. A total of 70 μL of 0.1 M calcium chloride ($CaCl_2$) was then added, followed by vortexing for 10 s. Then, 50 μL was deposited into sequential wells on a 96 well plate. At selected time points, each well was washed with 9 g/L saline solution to halt clotting. The liquid was immediately aspirated and washes repeated until the solution was clear, indicating removal of all soluble blood components. When testing the nanocomposites, the nanocomposites were injected *via* syringe into the base of the well plates, ensuring the entire bottom surface was coated with gel. After a trial was complete, the final clotting time was marked in the well that formed a uniform clot, with no change in clot size in subsequent wells.

Quantification and Imaging of Interfacial Interactions. Anticoagulated whole blood was centrifuged for 2 min to separate red blood cell-rich (RBC-rich) and RBC-poor phases in a mini centrifuge (6000 rpm). A liquid solution of fluorescently labeled nanoplatelet was mixed with the RBC-rich and -poor phases. Repeated spin downs and washings were performed to remove unbound nanoplatelets. Dilute solutions of RBC-rich/nanoplatelet and RBC-poor/nanoplatelet were mixed and deposited onto glass slides for imaging with a fluorescence microscope.

SAXS Method. Small Angle X-ray Scattering (SAXS) was performed at the NSLS at Brookhaven National Laboratory at beamline X27C. Samples were placed in a 1 mm thick washer and sealed between Kapton tape. Samples were equilibrated at 37 and 20 °C for 20 min prior to collection of data. Scattering patterns were collected for 30 s per sample. Radial integration of the two-dimensional scattering pattern was performed to yield a one-dimensional scattering curve, which was corrected for empty cell and dark field scattering. Thin disk form factor model fitting was performed in MatLab using a nonlinear fit algorithm to fit the radius and a Gaussian distribution for polydispersity of the nanocomposite.

Thrombus Weight. Nanocomposite and powdered QuikClot samples were weighed into 2 mL Eppendorf tubes. Nanocomposites were centrifuged to standardize the surface area exposed. Citrated blood was reactivated by 10% (v/v) 0.1 M $CaCl_2$. A total of 100 μL of solution (10 μL $CaCl_2$ and 90 μL whole blood) was added to each Eppendorf tube. At each measured time point, clotting was stopped by addition of 200 μL sodium citrate solution (0.109 M). Any liquid was removed from the Eppendorf tube, leaving only clotted blood. The Eppendorf tubes were reweighed to determine the mass of clot produced in the tube. Clot mass was normalized to the area exposed to the nanocomposite. The same area was used for the commercial hemostat sample.

Cell Studies. Mouse monocyte/macrophage RAW 264.7 cells were procured from the ATCC. RAW 264.7 cells were grown in Dulbecco's Modified Eagle's Medium (DMEM) supplemented with 10% FBS and 1% penicillin/streptomycin at 37 °C in 5% CO_2. Lipopolysaccharide (LPS) was obtained from InvivoGen. RAW 264.7 macrophages were suspended in different formulations of gelatin and silicate at a concentration of 3×10^6 cells/mL and plated at a density of 2000 cells/well and grown for 24 hours. As controls, RAW cells were untreated or treated with 100 ng/mL of LPS. An ELISA assay (SA Biosciences) was performed according to the manufacturer's protocol on the supernatants of different groups to quantify the secreted cytokines IL-6 and TNF-α by the RAW cells. In another study, the cell viability of RAW cells in the presence of gelatin and silicate for 24 hours was measured with Cell Titer 96 Aqueous Non-Radioactive Cell Proliferation MTS Assay (Promega) according to manufacturer's protocol using a plate reader at 490 nm absorbance. To eliminate possible absorbance from silicate or gelatin components, the absorbance values with gelatin, silicate and nanocomposite hydrogels, without cells, were measured. These absorbance values were subtracted from the corresponding absorbance values for gelatin, silicate and nanocomposite hydrogels, with cells. This resulted in reading the absorbance values of only viable cells. Each tested hydrogel was measured in three separate wells.

***In Vivo* Experiments.** Male Wistar rats ($n = 20$; 200−250 g) were obtained from Charles River (Wilmington, MA), housed in the local animal care facility (PRB, Cambridge, MA) and fed *ad libitum*. Anesthesia and analgesia were achieved by isoflurane inhalation (2.0−2.5%) and subcutaneous carprofen administration (5 mg/kg/d). All experiments were conducted according to the NIH "Guide for the Care and Use of Laboratory Animals", and approved by the local animal care committee (HMA Standing Committee on Animals; protocol number 05055).

For subcutaneous implantation procedures (n = 8 rats), dorsal skin incisions (1 cm in length) were conducted, a small subcutaneous pocket was generated by blunt preparation, and nanocomposite gels (n = 8; 200 μL) were injected or QuikClot samples (n = 8; 200 μL) were implanted, respectively. The wounds were anatomically closed, and the animals were allowed to recover from anesthesia. After 3 and 28 days, the animals were euthanized by CO_2 inhalation, and the implants as well as adjacent tissue were explanted and further processed for histological analyses.

In the liver bleeding experiments (n = 12 rats), median laparotomy was performed and the central liver lobe was exposed. After draping of the surrounding *situs* with filter paper for blood collection, a standardized circular liver laceration was created by gluing a plastic disc (d = 10 mm) to the surface and superficially excising this area with a blade. Immediately after the injury, nanocomposite gel ($n = 5$; 200 μL) or QuikClot ($n = 2$; 200 μL) was applied on the site of lesion. Five minutes after the bleeding had been stopped, the abdomen was anatomically closed, and the animals were allowed to recover from anesthesia. After 28 days, the animals were euthanized by CO_2 inhalation, and the site of injury was inspected. To examine the principal lethality of the liver bleeding model, control rats (n = 5) underwent liver injury without subsequent application of a hemostat. In all liver bleeding experiments, the amount of bleeding was determined by weighing the blood-soaked filter papers after removal.

Histological analyses were conducted as previously published.[52] In brief, paraformaldehyde-fixed cryosections (6 μm) of all explants were stained with hematoxylin/eosin and microscopically analyzed.

Conflict of Interest: The authors declare no competing financial interest.

Supporting Information Available: Additional rheological analysis of hydrogel, SAXS curves, images of *in vivo* methodology, cell cytocompatibility. This material is available free of charge *via* the Internet at http://pubs.acs.org.

Acknowledgment. SAXS experiments were performed at Beamline X27C of the National Synchrotron Light Source at Brookhaven National Laboratory. This research was supported by the U.S. Army Research Office under contract W911NF-13-D-0001. R. K. Avery was supported by an NIH Interdepartmental Biotechnology Training Program (NIH/NIGMS 5T32GM008334). A. Paul acknowledges postdoctoral award from FRQS (Fonds de recherche du Québec - Santé), Quebec, Canada. A. Assmann acknowledges a postdoctoral award from the German Heart Foundation, Frankfurt, Germany.

REFERENCES AND NOTES

1. Ostomel, T. A.; Shi, Q.; Stucky, G. D. Oxide Hemostatic Activity. *J. Am. Chem. Soc.* **2006**, *128*, 8384–8385.
2. Spotnitz, W. D.; Burks, S. Hemostats, Sealants, and Adhesives: Components of the Surgical Toolbox. *Transfusion* **2008**, *48*, 1502–1516.
3. Dowling, M. B.; Kumar, R.; Keibler, M. A.; Hess, J. R.; Bochicchio, G. V.; Raghavan, S. R. A Self-Assembling Hydrophobically Modified Chitosan Capable of Reversible Hemostatic Action. *Biomaterials* **2011**, *32*, 3351–3357.
4. Baker, S. E.; Sawvel, A. M.; Zheng, N.; Stucky, G. D. Controlling Bioprocesses with Inorganic Surfaces: Layered Clay Hemostatic Agents. *Chem. Mater.* **2007**, *19*, 4390–4392.
5. Ruan, L.; Zhang, H.; Luo, H.; Liu, J.; Tang, F.; Shi, Y.-K.; Zhao, X. Designed Amphiphilic Peptide Forms Stable Nanoweb, Slowly Releases Encapsulated Hydrophobic Drug, and Accelerates Animal Hemostasis. *Proc. Natl. Acad. Sci. U.S. A.* **2009**, *106*, 5105–5110.
6. Burnett, L. R.; Richter, J. G.; Rahmany, M. B.; Soler, R.; Steen, J. A.; Orlando, G.; Abouswareb, T.; Van Dyke, M. E. Novel Keratin (Kerastat) and Polyurethane (Nanosan®-Sorb) Biomaterials Are Hemostatic in a Porcine Lethal Extremity Hemorrhage Model. *J. Biomater. Appl.* **2014**, *28*, 869–879.
7. Hildenbrand, T. A New Gelatine-Based Hemostat for Sinonasal Surgery: A Clinical Survey. *In Vivo* **2013**, *27*, 523–526.
8. Oz, M. C.; Rondinone, J. F.; Shargill, N. S. Floseal Matrix. *J. Card. Surg.* **2003**, *18*, 486–493.
9. Xie, X.; Tian, J.-k.; Lv, F.-q.; Wu, R.; Tang, W.-b.; Luo, Y.-k.; Huang, Y.-q.; Tang, J. A Novel Hemostatic Sealant Composed of Gelatin, Transglutaminase and Thrombin Effectively Controls Liver Trauma-Induced Bleeding in Dogs. *Acta Pharmacol. Sin.* **2013**, *34*, 983–988.
10. Ekenseair, A. K.; Boere, K. W. M.; Tzouanas, S. N.; Vo, T. N.; Kasper, F. K.; Mikos, A. G. Structure−Property Evaluation of Thermally and Chemically Gelling Injectable Hydrogels for Tissue Engineering. *Biomacromolecules* **2012**, *13*, 2821–2830.
11. Lu, H. D.; Soranno, D. E.; Rodell, C. B.; Kim, I. L.; Burdick, J. A. Secondary Photocrosslinking of Injectable Shear-Thinning Dock-and-Lock Hydrogels. *Adv. Healthcare Mater.* **2013**, *2*, 1028–1036.
12. Ostomel, T. A.; Shi, Q.; Stoimenov, P. K.; Stucky, G. D. Metal Oxide Surface Charge Mediated Hemostasis. *Langmuir* **2007**, *23*, 11233–11238.
13. Cha, C.; Shin, S. R.; Annabi, N.; Dokmeci, M. R.; Khademhosseini, A. Carbon-Based Nanomaterials: Multifunctional Materials for Biomedical Engineering. *ACS Nano* **2013**, *7*, 2891–2897.
14. Gaharwar, A. K.; Peppas, N. A.; Khademhosseini, A. Nanocomposite Hydrogels for Biomedical Applications. *Biotechnol. Bioeng.* **2014**, *111*, 441–453.
15. Schexnailder, P.; Schmidt, G. Nanocomposite Polymer Hydrogels. *Colloid Polym. Sci.* **2009**, *287*, 1–11.
16. Shin, S. R.; Bae, H.; Cha, J. M.; Mun, J. Y.; Chen, Y.-C.; Tekin, H.; Shin, H.; Farshchi, S.; Dokmeci, M. R.; Tang, S.; *et al.* Carbon Nanotube Reinforced Hybrid Microgels as Scaffold Materials for Cell Encapsulation. *ACS Nano* **2011**, *6*, 362–372.
17. Shin, S. R.; Jung, S. M.; Zalabany, M.; Kim, K.; Zorlutuna, P.; Kim, S. b.; Nikkhah, M.; Khabiry, M.; Azize, M.; Kong, J.; *et al.* Carbon-Nanotube-Embedded Hydrogel Sheets for Engineering Cardiac Constructs and Bioactuators. *ACS Nano* **2013**, *7*, 2369–2380.
18. Dobrovolskaia, M. A.; McNeil, S. E. Immunological Properties of Engineered Nanomaterials. *Nat. Nanotechnol.* **2007**, *2*, 469–478.
19. Jones, C. F.; Grainger, D. W. *In Vitro* Assessments of Nanomaterial Toxicity. *Adv. Drug Delivery Rev.* **2009**, *61*, 438–456.
20. Radomski, A.; Jurasz, P.; Alonso-Escolano, D.; Drews, M.; Morandi, M.; Malinski, T.; Radomski, M. W. Nanoparticle-Induced Platelet Aggregation and Vascular Thrombosis. *Br. J. Pharmacol.* **2005**, *146*, 882–893.
21. Semberova, J.; De Paoli Lacerda, S. H.; Simakova, O.; Holada, K.; Gelderman, M. P.; Simak, J. Carbon Nanotubes Activate Blood Platelets by Inducing Extracellular Ca^{2+} Influx Sensitive to Calcium Entry Inhibitors. *Nano Lett.* **2009**, *9*, 3312–3317.
22. Singh, S. K.; Singh, M. K.; Nayak, M. K.; Kumari, S.; Shrivastava, S.; Grácio, J. J.; Dash, D. Thrombus Inducing Property of Atomically Thin Graphene Oxide Sheets. *ACS Nano* **2011**, *5*, 4987–4996.
23. Gaharwar, A. K.; Mihaila, S. M.; Swami, A.; Patel, A.; Sant, S.; Reis, R. L.; Marques, A. P.; Gomes, M. E.; Khademhosseini, A. Bioactive Silicate Nanoplatelets for Osteogenic Diffrentiation of Human Human Mesenchymal Stem Cells. *Adv. Mater.* **2013**, *25*, 3329–3336.
24. Ruzicka, B.; Zaccarelli, E. A Fresh Look at the Laponite Phase Diagram. *Soft Matter* **2011**, *7*, 1268–1286.
25. Viseras, C.; Cerezo, P.; Sanchez, R.; Salcedo, I.; Aguzzi, C. Current Challenges in Clay Minerals for Drug Delivery. *Appl. Clay Sci.* **2010**, *48*, 291–295.
26. Gaharwar, A. K.; Kishore, V.; Rivera, C.; Bullock, W.; Wu, C. J.; Akkus, O.; Schmidt, G. Physically Crosslinked Nanocomposites from Silicate-Crosslinked Peo: Mechanical Properties and Osteogenic Differentiation of Human Mesenchymal Stem Cells. *Macromol. Biosci.* **2012**, *12*, 779–793.
27. Gaharwar, A. K.; Rivera, C.; Wu, C.-J.; Chan, B. K.; Schmidt, G. Photocrosslinked Nanocomposite Hydrogels from Peg and Silica Nanospheres: Structural, Mechanical and Cell Adhesion Characteristics. *Mater. Sci. Eng., C* **2013**, *33*, 1800–1807.
28. Gaharwar, A. K.; Schexnailder, P.; Kaul, V.; Akkus, O.; Zakharov, D.; Seifert, S.; Schmidt, G. Highly Extensible Bio-Nanocomposite Films with Direction-Dependent Properties. *Adv. Funct. Mater.* **2010**, *20*, 429–436.
29. Gaharwar, A. K.; Schexnailder, P. J.; Kline, B. P.; Schmidt, G. Assessment of Using Laponite Cross-Linked Poly(ethylene oxide) for Controlled Cell Adhesion and Mineralization. *Acta Biomater.* **2011**, *7*, 568–577.
30. Arnaud, F.; Parreno-Sadalan, D.; Tomori, T.; Delima, M. G. Teranishi, K.; Carr, W.; McNamee, G.; McKeague, A.; Govindaraj, K.; Beadling, C. Comparison of 10 Hemostatic Dressings in a Groin Transection Model in Swine. *J. Trauma Acute Care Surg.* **2009**, *67*, 848–855.
31. Bowman, P. D.; Wang, X.; Meledeo, M. A.; Dubick, M. A.; Kheirabadi, B. S. Toxicity of Aluminum Silicates Used in Hemostatic Dressings toward Human Umbilical Veins Endothelial Cells, HeLa Cells, and Raw267.4 Mouse Macrophages. *J. Trauma Acute Care Surg.* **2011**, *71*, 727–732.
32. Carretero, M. I.; Pozo, M. Clay and Non-Clay Minerals in the Pharmaceutical and Cosmetic Industries Part II. Active Ingredients. *Appl. Clay Sci.* **2010**, *47*, 171–181.
33. Nelson O'Donoghue, M. Eye Cosmetics. *Dermatol. Clin.* **2000**, *18*, 633–639.
34. Ashby, N.; Binks, B. Pickering Emulsions Stabilised by Laponite Clay Particles. *Phys. Chem. Chem. Phys.* **2000**, *2*, 5640–5646.
35. Thompson, D. W.; Butterworth, J. T. The Nature of Laponite and Its Aqueous Dispersions. *J. Colloid Interface Sci.* **1992**, *151*, 236–243.
36. Gaharwar, A. K.; Schexnailder, P. J.; Dundigalla, A.; White, J. D.; Matos-Pérez, C. R.; Cloud, J. L.; Seifert, S.; Wilker, J. J.; Schmidt, G. Highly Extensible Bio-Nanocomposite Fibers. *Macromol. Rapid Commun.* **2011**, *32*, 50–57.
37. Wu, C.-J.; Gaharwar, A. K.; Schexnailder, P. J.; Schmidt, G. Development of Biomedical Polymer-Silicate Nanocomposites: A Materials Science Perspective. *Materials* **2010**, *3*, 2986–3005.
38. Pawar, N.; Bohidar, H. Surface Selective Binding of Nanoclay Particles to Polyampholyte Protein Chains. *J. Chem. Phys.* **2009**, *131*, 045103.
39. Stevens, K. R.; Einerson, N. J.; Burmania, J. A.; Kao, W. J. *In Vivo* Biocompatibility of Gelatin-Based Hydrogels and Interpenetrating Networks. *J. Biomater. Sci., Polym. Ed.* **2002**, *13*, 1353–1366.
40. Bohidar, H. B.; Jena, S. S. Kinetics of Sol-Gel Transition in Thermoreversible Gelation of Gelatin. *J. Chem. Phys.* **1993**, *98*, 8970–8977.
41. Jorge, M. F. C.; Flaker, C. H. C.; Nassar, S. F.; Moraes, I. C. F.; Bittante, A. M. Q. B.; Sobral, P. J. d. A. Viscoelastic and

Rheological Properties of Nanocomposite-Forming Solutions Based on Gelatin and Montmorillonite. *J. Food Eng.* **2014**, *120*, 81–87.
42. Pedersen, J. S. Analysis of Small-Angle Scattering Data from Colloids and Polymer Solutions: Modeling and Least-Squares Fitting. *Adv. Colloid Interface Sci.* **1997**, *70*, 171–210.
43. Olsen, B. D.; Kornfield, J. A.; Tirrell, D. A. Yielding Behavior in Injectable Hydrogels from Telechelic Proteins. *Macromolecules* **2010**, *43*, 9094–9099.
44. Davie, E. W.; Ratnoff, O. D. Waterfall Sequence for Intrinsic Blood Clotting. *Science* **1964**, *145*, 1310–1312.
45. de la Torre, R. A.; Bachman, S. L.; Wheeler, A. A.; Bartow, K. N.; Scott, J. S. Hemostasis and Hemostatic Agents in Minimally Invasive Surgery. *Surgery* **2007**, *142*, S39–S45.
46. Bertram, J. P.; Williams, C. A.; Robinson, R.; Segal, S. S.; Flynn, N. T.; Lavik, E. B. Intravenous Hemostat: Nanotechnology To Halt Bleeding. *Sci. Transl. Med.* **2009**, *1*, 11ra22.
47. Wagner, W. R.; Pachence, J. M.; Ristich, J.; Johnson, P. C. Comparative *in Vitro* Analysis of Topical Hemostatic Agents. *J. Surg. Res.* **1996**, *66*, 100–108.
48. Roach, P.; Farrar, D.; Perry, C. C. Interpretation of Protein Adsorption: Surface-Induced Conformational Changes. *J. Am. Chem. Soc.* **2005**, *127*, 8168–8173.
49. Wojciechowski, P.; Ten Hove, P.; Brash, J. L. Phenomenology and Mechanism of the Transient Adsorption of Fibrinogen from Plasma (Vroman Effect). *J. Colloid Interface Sci.* **1986**, *111*, 455–465.
50. Okamoto, Y.; Yano, R.; Miyatake, K.; Tomohiro, I.; Shigemasa, Y.; Minami, S. Effects of Chitin and Chitosan on Blood Coagulation. *Carbohydr. Polym.* **2003**, *53*, 337–342.
51. Zhang, J.; Xia, W.; Liu, P.; Cheng, Q.; Tahi, T.; Gu, W.; Li, B. Chitosan Modification and Pharmaceutical/Biomedical Applications. *Mar. Drugs* **2010**, *8*, 1962–1987.
52. Assmann, A.; Delfs, C.; Munakata, H.; Schiffer, F.; Horstkotter, K.; Huynh, K.; Barth, M.; Stoldt, V. R.; Kamiya, H.; Boeken, U.; *et al.* Acceleration of Autologous *in Vivo* Recellularization of Decellularized Aortic Conduits by Fibronectin Surface Coating. *Biomaterials* **2013**, *34*, 6015–6026.